Phase evolution in the ferroelectric relaxor Ba(Ti$_{1-x}$, Zr$_x$)O$_3$ from atomistic simulations

C. Mentzer, S. Lisenkov, Z. G. Fthenakis, and I. Ponomareva

Department of Physics, University of South Florida, Tampa, Florida 33620, USA

We develop and/or use a combination of first-principles density functional theory and first-principles-based effective Hamiltonian approaches to investigate phase evolution in Ba(Ti$_{1-x}$, Zr$_x$)O$_3$ ferroelectric relaxor. Our simulations reveal two competing effects, which are associated with substitution of Ti with Zr and primarily responsible for the unusual phase evolution and the properties of this family of solid solutions. They are the negative chemical pressure that Zr exerts on the BaTiO$_3$ matrix and the ferroelectric "inactivity" of Zr itself. While the former has a stabilizing effect on ferroelectricity, the latter disrupts the ferroelectric cooperation. These competing effects are responsible for the so-called pinched phase transition, where the three phases of parent BaTiO$_3$ merge together, and the loss of ferroelectricity at the onset of relaxor behavior. The origin of the controversial diffuse phase transition is attributed to the coexistence of the three ferroelectric phases. In the region of the diffuse phase transition, we detect polar nanoregions, which often exhibit unusual nanopillar geometry.

I. INTRODUCTION

Ferroelectric solid solutions such as Pb(Ti$_{1-x}$, Zr$_x$)O$_3$, Ba(Ti$_{1-x}$, Zr$_x$)O$_3$, and (Ba$_{1-x}$, Sr$_x$)TiO$_3$ exhibit excellent ferroelectric, pyroelectric, and piezoelectric properties and find numerous applications in capacitors, nonlinear optical devices, piezoelectric transducers, ultrasonic imaging, common rail fuel injection systems, energy harvesting devices, just to name a few [1,2]. Their unique feature is the high tunability of these properties by varying concentration. Among different solid solutions, the family of Ba(Ti$_{1-x}$, Zr$_x$)O$_3$ solid solutions stands out because of their lead-free nature and the extreme richness of the phase diagram. The parent compound BaTiO$_3$ exhibits a sequence of phase transitions: paraelectric cubic to ferroelectric tetragonal at 393 K, ferroelectric tetragonal to ferroelectric orthorhombic at 278 K, and ferroelectric orthorhombic to ferroelectric rhombohedral at 183 K [3]. As the Zr concentration in these compounds increases, the multiple phase transitions of parent BaTiO$_3$ merge, giving rise to the so-called pinched transition around $x = 0.10$ [3] [see Fig. 4(b)]. Interestingly, while the existence of a pinched transition region is well established experimentally, there is a lack of microscopic understanding of the driving force behind the phase transitions merging. How does paraelectric BaZrO$_3$ stabilize the ferroelectric rhombohedral phase? In contrast, in other BaTiO$_3$-based solid solutions, such as (Ba$_{1-x}$, Sr$_x$)TiO$_3$, the transition temperatures for all three ferroelectric phase transitions decrease gradually with the increase of SrTiO$_3$ content [4,5].

In a concentration range of 0.10–0.20, Ba(Ti$_{1-x}$, Zr$_x$)O$_3$ undergoes a single phase transition from the paraelectric cubic to the ferroelectric rhombohedral phase. However, the associated peak in the dielectric susceptibility is much broader than in BaTiO$_3$, which sometimes is referred to as the diffuse phase transition [3]. The nature of the diffuse phase transition is rather controversial, as some believe that such a transition is the signature of the relaxor state [6], while other

experimental evidence suggests that the diffuse phase transition is actually associated with a ferroelectric phase transition due to the observation of the ferroelectric domains in the vicinity of the temperature T_m associated with the maximum in the dielectric constant [7]. At higher substitutions of >0.20 of Zr, T_m shows a frequency dependence, which is a hallmark of relaxor behavior. Such a signature property of relaxors is attributed to the existence of polar nanoregions (PNRs), which are nanoscopic regions of locally correlated polarization that appear at the "Burns" temperature. The microscopic origins of PNRs are typically related to the structural and charge inhomogeneities present in relaxors. However, the onset of relaxor behavior in systems without nominal charge disorder, such as in Ba(Ti$_{1-x}$, Zr$_x$)O$_3$, is not well understood [3]. It is believed that a broad distribution of PNR sizes and their dynamical nature give rise to a broad distribution of relaxation times and consequently a broad dielectric response. In Ba(Ti$_{1-x}$, Zr$_x$)O$_3$ in the compositional range 0.25–0.35 of Zr, a percolation transition occurs below a temperature associated with the freezing of polar nanoregions. In the range of x from 0.35 to 0.80, canonical nonergodic relaxor behavior occurs with macroscopic cubic symmetry.

Clearly addressing these questions and controversies at the fundamental level requires atomistic insights from first-principles-based finite-temperature dynamical simulations. In a recent study [8], a first-principles-based approach was developed to investigate Ba(Ti$_{1-x}$, Zr$_x$)O$_3$ solid solutions with $x = 0.5$. The static simulations indicated that the random fields and random strains do not play a major role in the relaxor behavior of this solid solution. The study attributed the relaxor state to the difference in the ferroelectric strength between Ti and Zr ions as well as the importance of antiferroelectric-like interactions. A follow-up study revealed a field-induced percolation of polar nanoregions in this material [9]. In contrast, another recent atomistic study looked at the dynamics of relaxor 75%PbMg$_{1/3}$Nb$_{2/3}$O$_3$-25%PbTiO$_3$

and proposed a model of anisotropic local correlations that contradicts the polar nanoregion model [10]. The study of high-frequency dynamics in $Ba(Ti_{1-x}, Zr_x)O_3$ led to the prediction of an exotic fanoresonance [11]. More recently, some $Ba(Ti_{1-x}, Zr_x)O_3$ solid solutions were studied at 0 K with first-principles simulations [12]. It was found that Zr substitution of Ti strongly favors short-range repulsive force. On the other hand, the bigger size of Zr locally favors the long-range interactions along O-Ti-O-Ti-O chains. At the same time, to the best of our knowledge, no microscopic insight is available for the region associated with the crossover between the ferroelectric, diffuse ferroelectric, and relaxor state, which is, in our opinion, instrumental in understanding the relaxor state in systems without nominal charge disorder.

The aims of this work are (i) to develop a first-principles-based computational approach capable of modeling this family of solid solutions in a wide compositional and temperature range; (ii) to apply this computational approach along with first-principles 0 K simulations to elucidate the phase evolution in these solid solutions; and (iii) to address some of the aforementioned questions and controversies.

II. METHODOLOGY

We begin by investigating two compositions of $Ba(Ti_{1-x}, Zr_x)O_3$, $x = 0.0$ and 0.125, at 0 K using first-principles density functional theory (DFT) calculations. The Vienna simulation package (VASP) [13] was used with the projector augmented wave method [14]. The Kohn-Sham equations were solved using the local density approximation. We used a cutoff energy of 500 eV, which yielded good convergence. For electronic structure calculation, an $8 \times 8 \times 8$ Monkhorst-Pack mesh was chosen. The simulation supercell contained $2 \times 2 \times 2$ cubic perovskite unit cells of $BaTiO_3$. For $Ba(Ti_{0.875}, Zr_{0.125})O_3$, one of the Ti in the supercell was replaced with Zr.

All structural optimizations of the supercells were carried out until the forces on the ions were less than 10^{-4} eV/Å and the stresses were less than 0.1 kbar. Both structures were investigated in their cubic $Pm\bar{3}m$ phase and $R3m$ ground state. The polarization was calculated using the Berry phase approach [15] and the ionic displacements. In the latter, the polarization was computed from $P = Z^* \Delta u/V$, where Z^* is the Born effective charge for the ions and u is half the ionic displacements associated with polarization reversal. We used the following values for the Born effective charges: $Z^*_{Ba} = 2.75$, $Z^*_{Zr} = 6.11$, $Z^*_{Ti} = 7.40$, $Z^*_{O1} = -5.82$, $Z^*_{O2} = -2.16$, which were found from DFT calculations. In the ground state of $BaTiO_3$ the polarization is aligned along the $\langle 111 \rangle$ crystallographic direction, and it has a value of 30.0 $\mu C/cm^2$ from Berry phase calculations and 31.8 $\mu C/cm^2$ from ionic displacements computations. These values compare well with the experimental value of 33.5 $\mu C/cm^2$ [16].

To elucidate the atomistic effect of Ti substitution with Zr, we replaced one of the Ti with Zr in both cubic and ground-state phases of the $BaTiO_3$, and we computed the associated forces that are shown schematically in Fig. 1. This corresponds to $Ba(Ti_{0.875}, Zr_{0.125})O_3$. In both the cubic and $R3m$ phases, Zr pushes surrounding atoms away due to its larger ionic size, which ultimately leads to the lattice
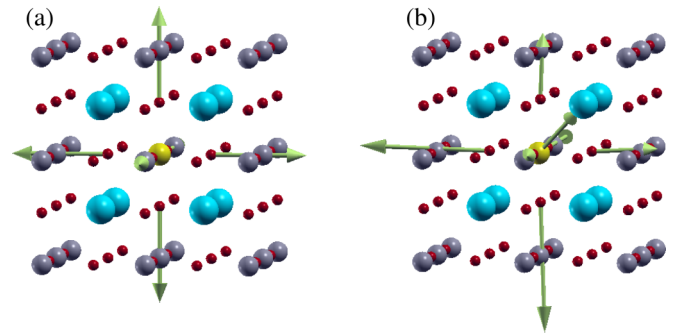

FIG. 1. Schematic representation of the forces acting on Zr substitution in $BaTiO_3$ cubic phase (a) and ground state (b).

expansion. In addition, in $R3m$ phase we find a relatively large force on Zr. The direction of the force indicates that this is a restoring force that acts to return Zr to its undistorted position, revealing its inability to polarize with the rest of the lattice. Next, both supercells were relaxed through optimization of ionic positions and supercell size. The resultant ionic displacements are consistent with the force patterns. In the cubic phase of $Ba(Ti_{0.875}, Zr_{0.125})O_3$ we find a 0.75% increase of the lattice constant with respect to $BaTiO_3$, which corresponds to -3.64 GPa pressure applied to $BaTiO_3$. Negative pressure has a stabilizing effect on ferroelectricity as it shifts the energy balance in favor of long-range Coulomb interactions. In $R3m$ phase of $Ba(Ti_{0.875}, Zr_{0.125})O_3$, the polarization is 26.0 $\mu C/cm^2$ from Berry phase calculations and 31.3 $\mu C/cm^2$ from the ionic displacements.

We have used the ionic displacements approach to compute local polarization in the $R3m$ phase of $Ba(Ti_{0.875}, Zr_{0.125})O_3$ and compare it to the one in $BaTiO_3$. The polarization vector was taken to be centered on the Ti or Zr site. The results are shown schematically in Fig. 2. The most prominent feature is the extremely small polarization on the Zr site (only $0.3P_{BTO}$), which confirms that Zr does not like to polarize. For the Zr nearest-neighbor unit cells along $\langle 100 \rangle$, the polarization direction deviates significantly from the $\langle 111 \rangle$ direction and is almost along $\langle 011 \rangle$. Interestingly, for Ti unit cells we find enhancement of local polarization in comparison with $BaTiO_3$ (about $1.12 P_{BTO}$).

Thus our simulations demonstrate that larger Zr pushes away its surrounding ions, which leads to the lattice expansion (chemical pressure). Zr, however, does not participate in the collective distortions of the $BaTiO_3$ lattice that give origin
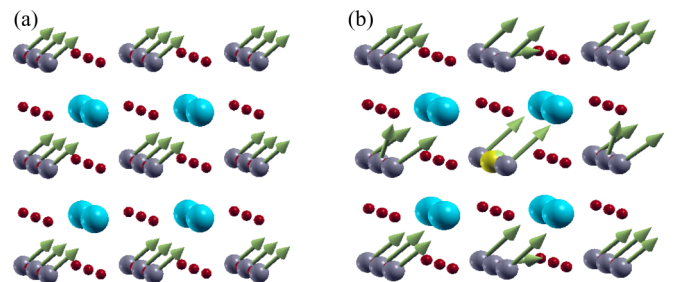

FIG. 2. Schematic representation of the local polarization in $BaTiO_3$ (a) and $Ba(Ti_{0.875}, Zr_{0.125})O_3$ (b).
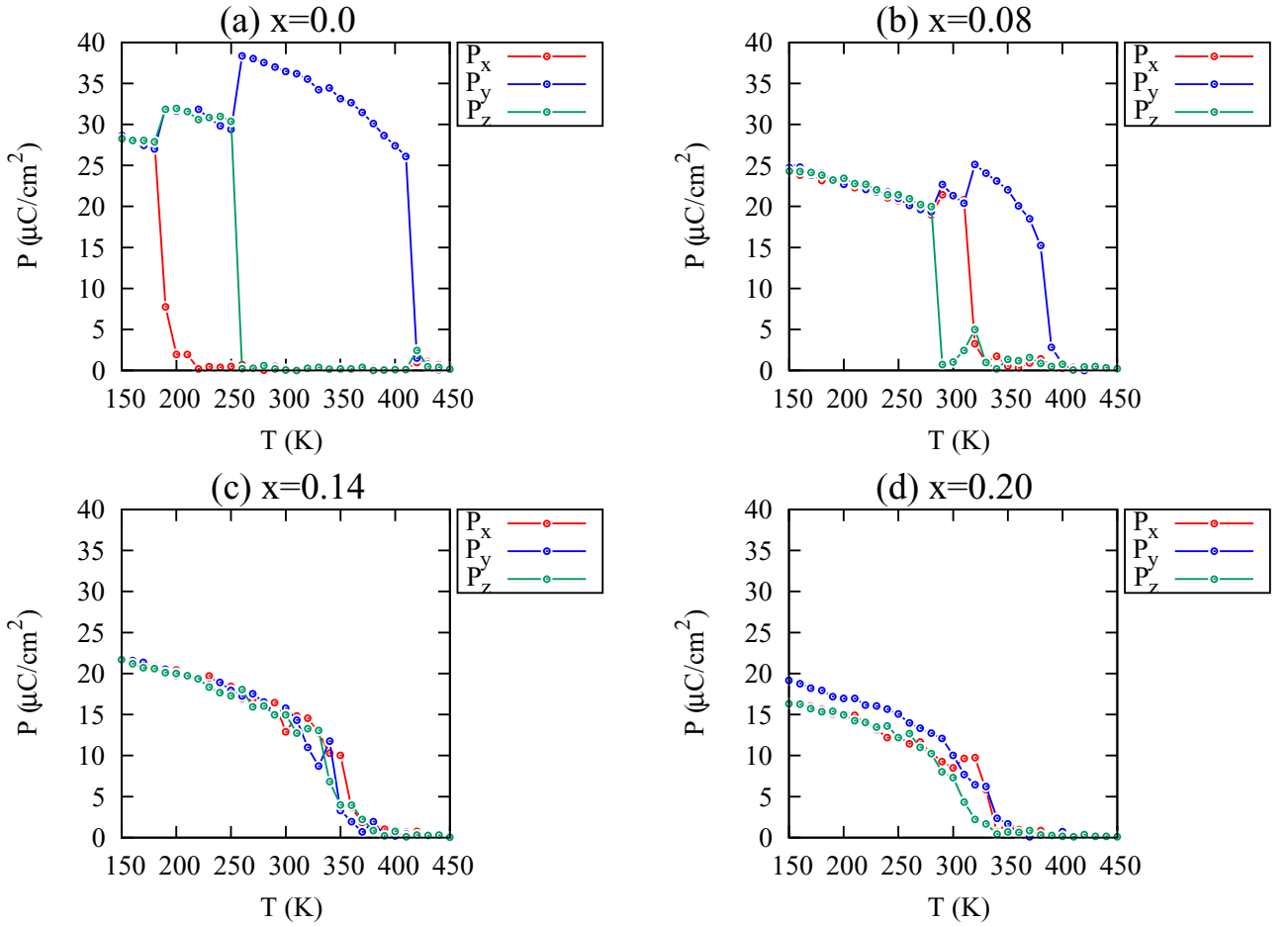
FIG. 3. Temperature evolution of polarization components for a few representative Zr concentrations.

to the polar phase. Quite surprisingly, Zr plays a dual role: it favors ferroelectricity through exerting negative chemical pressure on the BaTiO$_3$ matrix (mechanical effect), while simultaneously weakening the ferroelectric interactions by not participating in the collective distortion (electrostatic effect). These findings are in line with previous computational studies [8,12].

To study the phase evolution in a wide concentration range and at finite temperatures, we extend the first-principles-based effective Hamiltonian of Ref. [17] to the case of Ba(Ti$_{1-x}$, Zr$_x$)O$_3$ with low Zr concentration. The degrees of freedom for the Hamiltonian include local modes, $\mathbf{u}_i$, that are proportional to the dipole moment in the unit cell, and strain variable tensors, η_i (in Voigt notations), that are responsible for mechanical deformations of a unit cell. The energy of the Hamiltonian is [17]

$$E^{\text{tot}} = E^{\text{FE}}(\{\mathbf{u}_i\}) + E^{\text{elas}}(\{\eta_i\})$$
$$+ E^{\text{FE-elas}}(\{\mathbf{u}_i, \eta_i\}) + E^{\text{elec}}(\{\mathbf{u}_i\}), \quad (1)$$

where E^{FE} is the energy associated with the ferroelectric local modes and includes contributions from the dipole-dipole interactions, short-range interactions, and on-site self energy as defined in Ref. [18]. The second term, E^{elas}, is the elastic energy associated with the unit cell deformations. $E^{\text{FE-elas}}$ is the energy contribution due to the interactions between

the ferroelectric local modes and the strain. The last term, $E^{\text{elec}}(\{\mathbf{u}_i\}) = Z^* \sum_i \mathbf{E} \cdot \mathbf{u}_i$, gives the interaction energy between the local modes and an external electric field, $\mathbf{E}$.

To extend the Hamiltonian to the case of Ba(Ti$_{1-x}$, Zr$_x$)O$_3$, we recall that DFT calculations revealed that Zr does not participate in the collective displacement that gives origin to the spontaneous polarization in BaTiO$_3$. This means that if displaced, it experiences a restoring force. We computed the restoring force acting on the local mode centered on Zr as follows: $\mathbf{F}_{\mathbf{u}} = \sum_i (\mathbf{F}_i^{\text{rho}} - \mathbf{F}_i^{\text{cubic}})\xi_i$. Here $\mathbf{F}_i^{\text{rho}}$ and $\mathbf{F}_i^{\text{cubic}}$ are the forces on the ion i surrounding Zr in the $R3m$ and cubic phase, respectively. Zr itself is also included in the summation. These forces are obtained from DFT calculations. ξ_i are the components of the eigenvector associated with the unstable polar mode of BaTiO$_3$. They are $\xi_{\text{Ba}} = -0.25$, $\xi_{\text{Ti}} = -0.74$, $\xi_{\text{O}_1} = 0.52$, and $\xi_{\text{O}_2} = 0.24$ [19]. Note that we subtract forces acting on the ions in the cubic phase in order to separate the electrostatic and mechanical effects of Ti substitution. This force was then used to calculate the restoring force constant $k_{\text{Zr}} = -F_z/2u_z$, where u_z is the Cartesian component of the local mode. The associated harmonic term in the effective Hamiltonian is $\sum_j k_{\text{Zr}}[u_x^2(j) + u_y^2(j) + u_z^2(j)]$, where $k = 0.172\,13$ Ha/Bohr^2 and j runs over all unit cells that contain Zr.

To model the lattice expansion due to the presence of Zr, we simulate hydrostatic pressure that depends on Zr
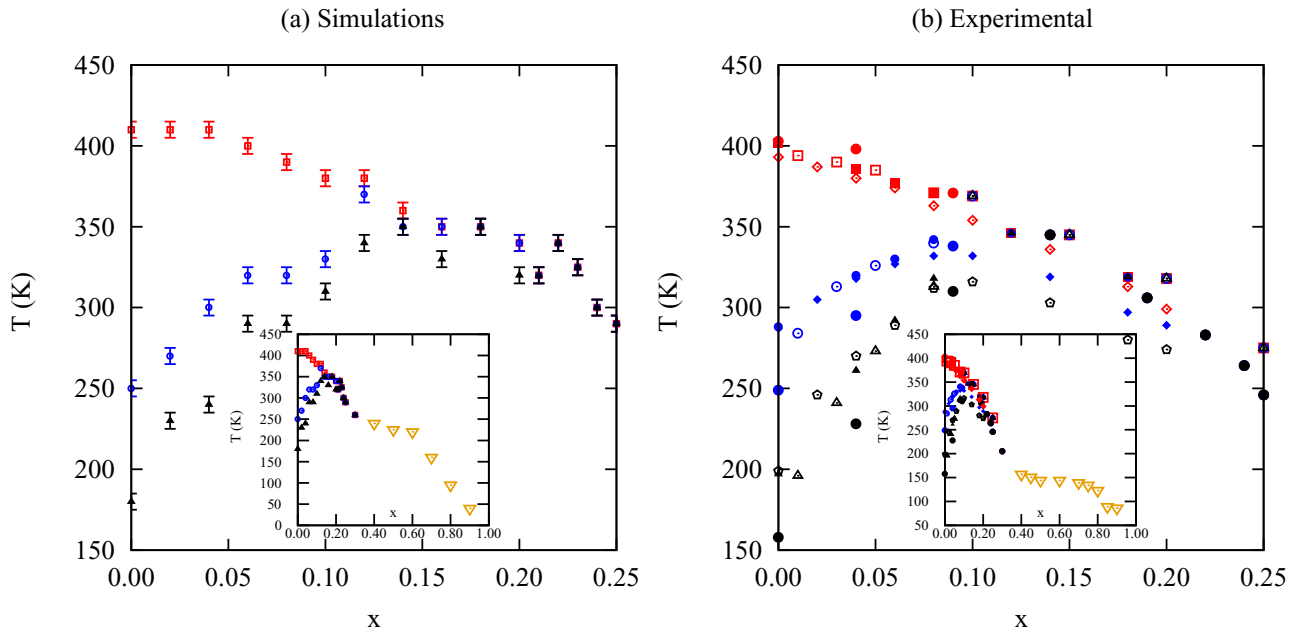
FIG. 4. Dependence of transition temperatures on Zr concentration obtained from computations (a), and experimental data from the literature [20–22] (b). The insets show the data in the entire concentration range. Yellow triangles in the inset show T_m.

concentration as follows: $P = -22 \times x$ GPa, which was found on the basis of first-principles calculations. More specifically, we ran DFT simulations with one through eight Ti ions replaced with Zr in a $2 \times 2 \times 2$ supercell to cover the entire compositional range. These simulations produced the equilibrium lattice constant as a function of Zr concentration, $a(x)$. The lattice constant was found to increase linearly with Zr concentration, in agreement with another DFT study [12]. Next a cubic lattice constant of $BaTiO_3$ was computed as a function of hydrostatic pressure, $a(P)$, in the range of 0 to -20 GPa. The data for $a(x)$ and $a(P)$ were used to compute the dependence of the negative pressure on Zr concentration.

The extended Hamiltonian was used in the framework of molecular dynamics (MD) to study the finite-temperature properties of $Ba(Ti_{1-x}, Zr_x)O_3$. Since many of the characteristic features of these solid solutions are believed to originate from dynamical and thermal fluctuations, we believe that MD is the appropriate tool for investigation of their properties. Supercell sizes of $12 \times 12 \times 12$, $20 \times 20 \times 20$, and $30 \times 30 \times 30$ were considered in order to address the effect of the supercell size. To trace the temperature evolution of the $Ba(Ti_{1-x}, Zr_x)O_3$ properties, the supercells were annealed from 450 K down to 10 K in steps of 10 K. Although we expect our approach to be accurate for low Zr concentrations, we nevertheless carried out simulations in the entire compositional range. Several sets of simulations were run with different numbers of MD steps: 40 000 MD steps (Set 1), 100 000 MD steps (Set 2), and 600 000 MD steps (Set 3), to investigate the dynamical aspect of the properties. While for pure $BaTiO_3$ we did not find significant differences in the data between $20 \times 20 \times 20$ and $30 \times 30 \times 30$ supercell sizes and between different simulation sets, this was not the case for $Ba(Ti_{1-x}, Zr_x)O_3$, where we found a dependence of the results on both the supercell size and the number of MD steps. In addition, the properties were also dependent on the particular

random distribution of Zr sites inside the $BaTiO_3$ matrix. This is an indication of the complexity of the energy landscape for these solid solutions.

III. RESULTS AND DISCUSSION

Figure 3 shows a few representative dependencies of polarization on temperature, $P(T)$, from our annealing simulations (Zr concentrations 0.00, 0.08, 0.14, and 0.20, Set 2). As Zr concentration increases, the Curie temperature decreases and the three ferroelectric transitions come closer together and merge, in agreement with experimental findings. The polarization decreases considerably in magnitude as Zr concentration increases. These data were used to obtain the dependence of the transition temperatures on Zr concentration, which is given in Fig. 4. Experimental data from the literature [20–22] are presented in the same figure. We find good agreement between the experimental and computational data. On the basis of the agreement, we conclude that the mechanical and electrostatic effects of Zr substitution of Ti identified from DFT calculations are primarily responsible for the phase evolution in these solid solutions. The insets to Fig. 4 show our computational data and experimental data from the literature in the entire compositional range. For $x > 0.30$ we find the macroscopically nonpolar phase with T_m decreasing with x, in striking agreement with experimental data.

To understand the microscopic origin for the observed features, we investigate the dipole patterns at 150 K obtained from Set 2. Some representatives are given in Fig. 5. For Zr concentrations below the one associated with a pinched transition, we find a polar matrix with some defectlike inclusions. In the concentration range 0.18–0.35 of Zr, we observe formations of nanoregions [Figs. 5(b)–5(d)] associated with different polarization orientations. Interestingly, however, some of these PNRs are not clusters but rather have
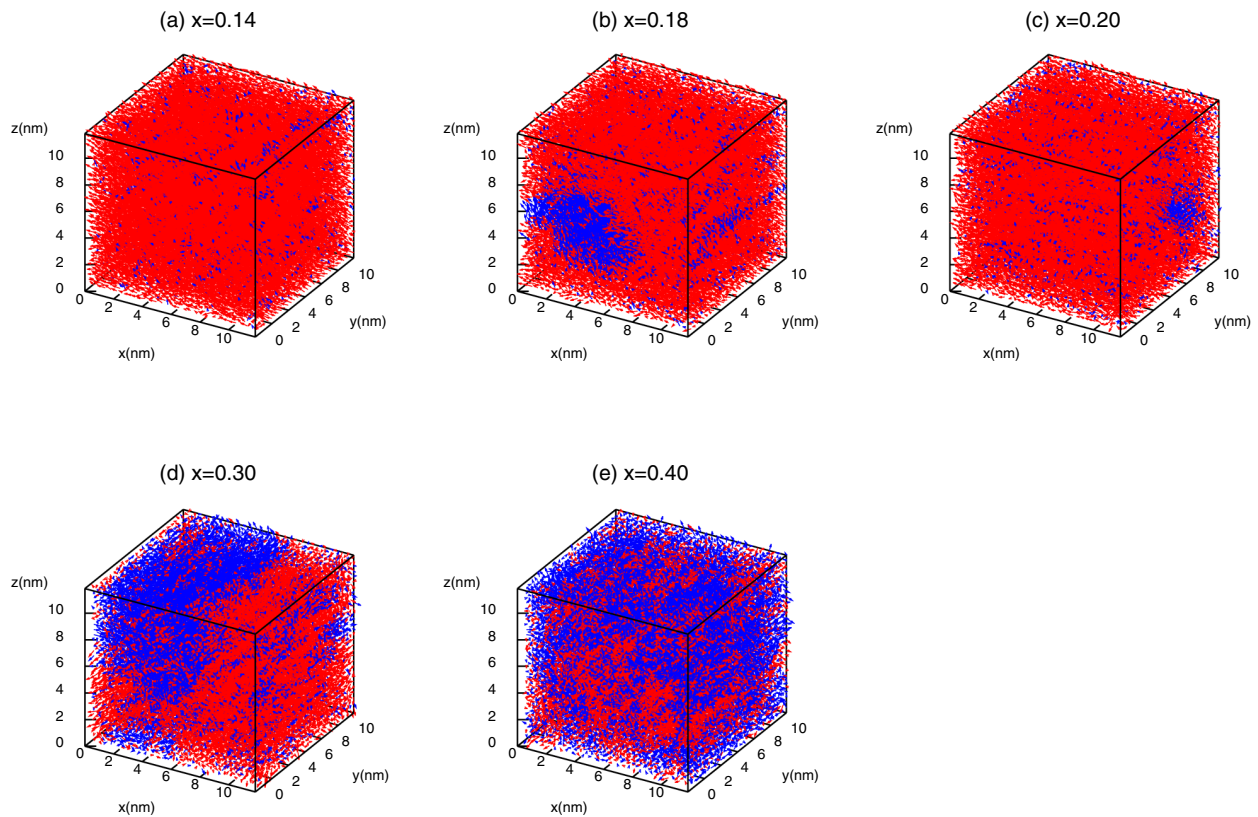
FIG. 5. Dipole patterns in the simulation supercells at 150 K. Different colors are used to visualize regions with polarization components of different directions.

a nanopillar geometry with the axis aligned along the $\langle 001 \rangle$ direction and extending through the entire supercell. This is in agreement with the experimental reports of one-dimensional PNRs with anisotropic chain dipoles along the $\langle 001 \rangle$ direction [23,24]. In some cases, we find an interpenetrating pattern of these nanopillars. Such clusters develop gradually as the temperature decreases below the Curie point. In simulations, the presence of such PNRs may lead to the apparent monoclinic phase due to the finite size of the supercell, as happens in Fig. 3(d). For Zr concentrations of 0.50 and above, the dipoles are completely disordered [see Fig. 5(e)].

Interestingly, we found that the precise details of the phase evolution and the phase diagram given in Figs. 3 and 4 depend on the number of MD steps, which suggests that in the vicinity of the phase transition the phases and PNRs evolve with time on a time scale of tenths of a nanosecond.

One of the open questions in ferroelectric relaxors is the nature of the diffuse phase transition. In $Ba(Ti_{1-x}, Zr_x)O_3$ it occurs for $0.15 \leqslant x \leqslant 0.20$. It was suggested [25] that the unusual behavior of the dielectric response in this region could be attributed to the overlapping of the three maxima in the dielectric response associated with the three ferroelectric phases (tetragonal, orthorhombic, and rhombohedral). Most puzzling, however, is the fact that these unusual features continue to persist even for Zr concentrations above the one associated with a pinched phase transition [25]. To investigate this, we study the response of $Ba(Ti_{1-x}, Zr_x)O_3$ with $x = 0.18$ to the applied ac electric field with a frequency of 1 GHz. We have simulated three different directions of the electric field: [100], [110], and [111] in the temperature range of

280–380 K, which brackets the Curie point of 350 K. A $30 \times 30 \times 30$ simulation supercell was used. The data for 280 and 320 K are given in Fig. 6. Surprisingly, we find that in this solid solution it is possible to stabilize any one of the three ferroelectric phases of the parent $BaTiO_3$, namely the tetragonal, orthorhombic, or rhombohedral phase. This is a manifestation of the fact that the free energies of these phases are rather close to each other. Furthermore, the possibility of switching between the different phases by the application of an electric field suggests high and rather unusual susceptibility, which could be responsible for the enhanced dielectric response. Such a property is extremely rare and highly desirable. Experimentally, it is expected to lead to the coexistence of all three ferroelectric phases [25]. Interestingly, we find that such phase competition occurs in the entire temperature range investigated, which could explain the enhancement of the dielectric response in a wide temperature range and the associated diffuse nature of the phase transition. Therefore, our data support the earlier hypothesis that the dielectric response in the region of the diffuse phase transition could be attributed to the overlapping of the three maxima in the dielectric response associated with the three ferroelectric phases [25].

IV. CONCLUSIONS

We have investigated phase evolution in $Ba(Ti_{1-x}, Zr_x)O_3$ solid solution using a combined first-principles DFT and first-principles-based effective Hamiltonian approach. From DFT computations, we found that Zr substitution of Ti leads to
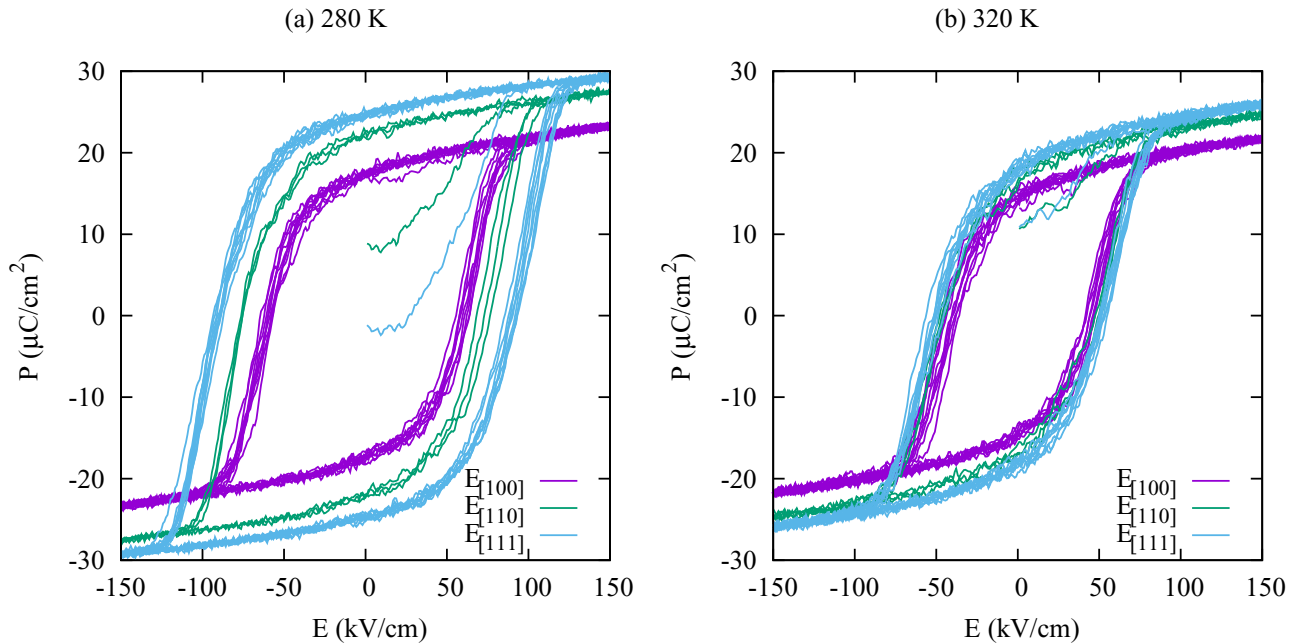
(a) 280 K

(b) 320 K

FIG. 6. The dependence of the polarization on the applied electric field for 280 K (a) and 320 K (b). The polarization component along the field direction is reported. The legend gives the direction of the applied electric field.

(i) lattice expansion of the $BaTiO_3$ matrix, which could be described as negative chemical pressure, and (ii) weakening of ferroelectric cooperation due to the inability of the Zr ion to undergo collective ferroelectric distortion. These findings were used to extend the effective Hamiltonian for $BaTiO_3$ to the case of $Ba(Ti_{1-x}, Zr_x)O_3$. Surprisingly, we found that the extended effective Hamiltonian predictions are in excellent agreement with the experimental phase diagram in the entire range of Zr concentration, which demonstrates that the two aforementioned effects of Ti substitution with Zr are primarily responsible for the phase evolution in this family of solid solutions. In particular, our methodology accurately predicts a pinched phase transition whose existence we attribute to the same competition between the stabilizing effect of negative chemical pressure and the destabilizing effect of "ferroelectrically nonactive" Zr. In the region of concentrations associated with the diffuse phase transition, we found PNRs with a different polarization direction. These nanoregions often have nanopillar geometry with the axis along the $\langle 001 \rangle$ direction. Furthermore, in this region we find that any one

of the three ferroelectric phases of the parent $BaTiO_3$ can occur, which could explain the enhanced susceptibility to the electric field (large and broad dielectric response). For concentrations $x > 0.30$, we find the macroscopically nonpolar phase with T_m decreasing with x. For concentrations $x > 0.50$, the dipoles are completely disordered in the absence of the electric field. We believe that our study advances the current understanding of the ferroelectric relaxors without nominal charge disorder, and the proposed computational methodology will allow for many future investigations into such solid solutions.

[1] K. Uchino, *Ferroelectric Devices* (Dekker, New York, 2000).

[2] S. R. Anton and H. A. Sodano, Smart Mater. Struct. **16**, R1 (2007).

[3] V. V. Shvartsman and D. C. Lupascu, J. Am. Ceram. Soc. **95**, 1 (2012).

[4] V. V. Lemanov, E. P. Smirnova, P. P. Syrnikov, and E. A. Tarakanov, Phys. Rev. B **54**, 3151 (1996).

[5] C. Ménoret, J. M. Kiat, B. Dkhil, M. Dunlop, H. Dammak, and O. Hernandez, Phys. Rev. B **65**, 224104 (2002).

[6] W. Xiaoyong, F. Yujun, and Y. Xi, Appl. Phys. Lett. **83**, 2031 (2003).

[7] V. V. Shvartsman, J. Zhai, and W. Kleemann, Ferroelectrics **379**, 77 (2009).

[8] A. R. Akbarzadeh, S. Prosandeev, E. J. Walter, A. Al-Barakaty, and L. Bellaiche, Phys. Rev. Lett. **108**, 257601 (2012).

[9] S. Prosandeev, D. Wang, A. R. Akbarzadeh, B. Dkhil, and L. Bellaiche, Phys. Rev. Lett. **110**, 207601 (2013).

[10] H. Takenaka, I. Grinberg, and A. M. Rappe, Phys. Rev. Lett. **110**, 147602 (2013).

[11] D. Wang, J. Hlinka, A. A. Bokov, Z. G. Ye, P. Ondrejkovic, J. Petzelt, and L. Bellaiche, Nat. Commun. **5**, 5100 (2014).

[12] D. Amoroso, A. Cano, and P. Ghosez, Phys. Rev. B **97**, 174108 (2018).

[13] G. Kresse and J. Furthmüller, Phys. Rev. B **54**, 11169 (1996).

[14] P. E. Blöchl, Phys. Rev. B **50**, 17953 (1994).

[15] R. D. King-Smith and D. Vanderbilt, Phys. Rev. B **47**, 1651 (1993).

[16] H. H. Wieder, Phys. Rev. **99**, 1161 (1955).

[17] R. Herchig, C.-M. Chang, B. K. Mani, and I. Ponomareva, Sci. Rep. **5**, 17294 (2015).

[18] W. Zhong, D. Vanderbilt, and K. M. Rabe, Phys. Rev. B **52**, 6301 (1995).

[19] For Zr we used ξ_{Ti}.

[20] J. Ravez, C. Broustera, and A. Simon, J. Mater. Chem. **9**, 1609 (1999).

[21] A. Peláiz-Barranco, Role of Ca off-centering in tuning ferroelectric phase transitions in Ba(Zr,Ti)O$_3$ system, in *Ferroelectric Materials: Synthesis and Characterization* (Rijeka: InTech, 2015).

[22] L. Dong, D. S. Stone, and R. S. Lakes, J. Appl. Phys. **111**, 084107 (2012).

[23] Y. Liu, R. L. Withers, X. Wei, and J. D. F. Gerald, J. Solid State Chem. **180**, 858 (2007).

[24] Y. Liu, R. L. Withers, B. Nguyen, and K. Elliott, Appl. Phys. Lett. **91**, 152907 (2007).

[25] D. Hennings, A. Schnell, and G. Simon, J. Am. Ceram. Soc. **65**, 539.